

# Identifying low-dimensional dynamics in Type-I edge-localised-mode processes in JET plasmas

F. A. Calderon,<sup>1, a)</sup> R. O. Dendy,<sup>2, 1</sup> S. C. Chapman,<sup>1</sup> A. J. Webster,<sup>2</sup> B. Alper,<sup>2</sup> R. M. Nicol,<sup>1</sup> and JET EFDA Contributors<sup>3, b)</sup>

<sup>1)</sup> *Centre for Fusion, Space and Astrophysics, Department of Physics, University of Warwick, Coventry, CV4 7AL, UK*

<sup>2)</sup> *EURATOM/CCFE Fusion Association, Culham Science Centre, Abingdon, OX14 3DB, UK*

<sup>3)</sup> *JET-EFDA, Culham Science Centre, Abingdon, OX14 3DB, UK*

(Dated: July 29, 2021)

Edge localised mode (ELM) measurements from reproducibly similar plasmas in the Joint European Torus (JET) tokamak, which differ only in their gas puffing rate, are analysed in terms of the pattern in the sequence of inter-ELM time intervals. It is found that the category of ELM defined empirically as Type I - typically more regular, less frequent, and having larger amplitude than other ELM types - embraces substantially different ELMing processes. By quantifying the structure in the sequence of inter-ELM time intervals using delay time plots, we reveal transitions between distinct phase space dynamics, implying transitions between distinct underlying physical processes. The control parameter for these transitions between these different ELMing processes is the gas puffing rate.

Keywords: tokamak edge plasmas, edge localised modes, nonlinear time series, delay time plots

## I. INTRODUCTION

Enhanced confinement operating regimes (H-mode) in magnetically confined plasmas are accompanied by pulses of energy and particle release known as edge localised modes (ELMs)<sup>1-6</sup>. At steady state, a magnetically confined tokamak plasma comprises a family of nested magnetic flux surfaces in a smooth, or laminar state. ELMing constitutes a relaxation process, for the edge region of H-mode plasmas, which encompasses an initial trigger for linear MHD instability evolving into a fully nonlinear detached state, such that structures propagate to the first wall where they generate recombination radiation. In parallel, local temperature and pressure gradients evolve rapidly. The onset of ELMing accompanies a sharp transition in the global state of the tokamak plasma, and changes in observed ELM character reflect changes in externally applied drive such as gas puffing and heating. Control, mitigation and prediction of the occurrence of large Type I ELMs are central challenges for magnetic confinement fusion plasma physics. There are many active experimental campaigns in this area<sup>7-9</sup>, particularly in support of the future ITER tokamak, for which the consequences of uncontrolled Type I ELMs may be unacceptable<sup>4,6</sup>. While successful theories for some component elements of the ELMing process have been constructed, there is currently no comprehensive first principles model that incorporates all of the physical effects that are known to contribute to the ELMing process. ELM categorisation is primarily

phenomenological<sup>3-5</sup>, furthermore it is not always easy to discriminate in real time between Type I and, say, Type III ELMing. Hitherto only a few papers<sup>10,11</sup> have addressed measured ELM sequences as the pulsed outputs of a nonlinear system, a field where generic analysis techniques are well developed and potential links to ELMing have long been apparent<sup>12</sup>. Characterisation of ELMing processes by applying dynamical systems theory to the data offers a fresh avenue to understanding, prediction and control, and may help identify some of the key properties that models for Type I ELMing must embody. Here we take the first steps.

D. Ruelle and F. Takens<sup>13</sup> initiated a classical scenario for the transition from ordered to disordered flow in fluids with increasing driving control parameter<sup>14,15</sup>. This has been observed in Rayleigh-Bénard convection in fluids<sup>16-20</sup>, and in drift wave turbulence<sup>21</sup> and flute instabilities in plasmas<sup>22</sup>. Oscillatory behaviour arises either if there is a constant of the motion, or if there is a limit cycle onto which the system dynamics is attracted in the presence of damping or dissipation. In the present case, where the system is the plasma undergoing the ELMing process, the nature and number of the relevant phase space co-ordinates is not known from first principles. Progress towards their identification can nevertheless be made by applying techniques of dynamical systems analysis to visualize changes in the topology of the phase space. A convenient method is that of ‘delay plots’, that is, to plot the successive time intervals between crossings of a surface of section in the phase space<sup>23-25</sup>.

In this article we report the application of delay plots to the measured time intervals or waiting times between successive ELMs. We consider ELM sequences from six similar plasmas in the JET tokamak, including JET plasma 57865 where the H-mode closely approaches an

<sup>a)</sup>Electronic mail: F.A.Calderon-Maldonado@warwick.ac.uk

<sup>b)</sup>See the Appendix of F. Romanelli *et al.*, Proceedings of the 23rd IAEA Fusion Energy Conference 2010, Daejeon, Korea.

ITER operating regime with respect to some, but not all, key dimensionless parameters<sup>26</sup>. We obtain evidence that Type I ELMing in these plasmas exhibits transitions between processes with distinct physical analogues, dependent on the value of the gas puffing rate as control parameter. In all six plasmas the toroidal magnetic field density is 2.7T, the plasma current is 2.5MA, neutral beam and ion cyclotron resonance heating power are 13.5MW and 2.0MW respectively, and the  $H_{98}$  confinement factor is in the range 0.87 to 1.0. In all six plasmas, gas puffing terminates at 23.3s and neutral beam heating is ramped down from 23.5 to 24.5s. The differences in Type I ELM character are largely determined by the different levels of externally applied gas puffing. The intensity of the  $D_\alpha$  signal, which sometimes saturates, is not necessarily a reliable proxy for the magnitude of the underlying ELM plasma phenomenon, whereas occurrence times are well defined. ELM occurrence and ELM waiting times are the primary physical indicators addressed in the present study. The moment of occurrence of each ELM is inferred from the  $D_\alpha$  datasets using an algorithm similar to that described in<sup>11</sup>, which exploits the steep leading edge of each ELM. This procedure generates a sequence of event times  $t_n$  for each  $n$ th ELM, and hence inter-event times  $\delta t_n = t_n - t_{n-1}$ . These sequences are used to construct delay plots, which are known<sup>23-25</sup> to capture aspects of the topology of the unknown underlying phase space evolution of the system.

## II. RESULTS AND DISCUSSIONS

Figures 1 and 2 show measured Type I ELM signals for a sequence of six JET H-mode plasmas 578nm, where  $nm$  is 72, 71, 70, 65, 67, and 69 in order of increasing magnitude and duration of the gas puffing rate, shown in Fig. 3, which is the key external control parameter. The upper trace in each panel of Figs. 1 and 2 plots the time-evolving intensity of Lyman alpha recombination radiation from deuterium,  $D_\alpha$ , measured by a camera directed at the inner divertor, normalised by the mean measured intensity. The two groupings of three plasmas are at lower (Fig. 1) and higher (Fig. 2) gas puffing rates. At lower gas puffing rates (Fig. 1) the ELM signal intensity is roughly the same across each time series, whereas at higher gas puffing rates (Fig. 2) this shows a rich structure. We will investigate this structure by sorting the ELM events that are used to construct the time series of inter-ELM time intervals (delay times), in terms of whether they exceed a threshold in signal intensity; the thresholds used are indicated by horizontal lines on the ELM time series (top panel in Figs 1 and 2). Each  $n$ th Type I ELM that has signal intensity exceeding a given threshold then forms a set of events at time  $t_n$  with the delay between events  $\delta t_n = t_n - t_{n-1}$ . The middle panels of Figs. 1 and 2 show the delay plots for a given threshold, that is,  $\delta t_{n+1}$  versus  $\delta t_n$ . The  $D_\alpha$  signal intensity for the ELM at  $t_n$  is indicated by colour

coding. These delay plots reflect the topology of the system phase space. For a trajectory that is approximately singly periodic the delay plot will exhibit a single concentration of points on the  $\delta t_{n+1} = \delta t_n$  line, centred on the mean period  $\tau = \delta t_{n+1} = \delta t_n$ . The spread of points about the mean period reflects a combination, in unknown proportions, of intrinsic and extrinsic sources of irregularity in a quasi-regular process, and determines the practical resolution limit of this method. A period-two oscillation will generate two concentrations of points, symmetrically placed either side of the  $\delta t_{n+1} = \delta t_n$  line. Dynamical switching between one period  $\tau_1$  and another at  $\tau_2$  will generate four concentrations of points: at the two distinct periods  $\tau_1$  and  $\tau_2$  on the  $\delta t_{n+1} = \delta t_n$  line, and at two locations symmetrically placed either side of the line, at  $(\delta t_{n+1}, \delta t_n)$  coordinates  $(\tau_1, \tau_2)$  and  $(\tau_2, \tau_1)$ .

The number of ELMs evaluated in these six JET plasmas ranges between 79 and 197. The mean inter-ELM time interval is in the range 25 to 60ms. The delay plots in Fig. 1 are insensitive to the threshold, in marked contrast to Fig. 2, suggesting that these reflect distinct processes. In Fig. 1, plasmas with successively greater gas puffing rates are shown from left to right. We can see that increased gas puffing causes the ELMing process to bifurcate from singly periodic (57872), via transitional behaviour (57871), to a situation where two periods are present (57870) together, with the plasma switching between them. This behaviour is approximately analogous to that of small amplitude oscillations of two weakly coupled pendulums with different natural frequencies. It is also apparent that a longer delay time  $\delta t_n$  before an ELM correlates statistically with a larger  $D_\alpha$  signal intensity. The bottom pair of plots in each panel of Figs. 1 and 2 displays the probability density functions (pdfs) for the distributions of measured  $\delta t_n$  for the ELM time series using the same amplitude thresholds as for the delay plots; in Fig. 1, unlike Fig. 2, these two panels are identical.

We now turn to Fig. 2 which corresponds to higher overall levels of gas puffing rate. It displays a transition in the ELMing process as the gas puffing rate is increased, which is different to that seen in Fig. 1. Each ELM with large  $D_\alpha$  signal intensity is statistically likely to be rapidly followed by a population of postcursor ELMs with smaller  $D_\alpha$  signal intensity. The likelihood of a postcursor ELM, and their number, increases with gas puffing rate. As a consequence, the delay plots constructed for different thresholds now, unlike Fig. 1, show different structure. At relatively low gas puffing rate (left hand plots) most delays fall within a single group on the  $\delta t_{n+1} = \delta t_n$  line. However when the threshold is reduced, smaller postcursor events begin to feature in the time series of delays and result in populations (lines parallel to the axes) far from the  $\delta t_{n+1} = \delta t_n$  line, and a new, narrowly constrained group on the  $\delta t_{n+1} = \delta t_n$  line at small  $(\delta t_{n+1}, \delta t_n)$ . As the gas puffing rate is increased, these small postcursor events come to dominate numerically. It is noteworthy that whereas ELMs with large signal amplitude exhibit a broad inter-ELM time

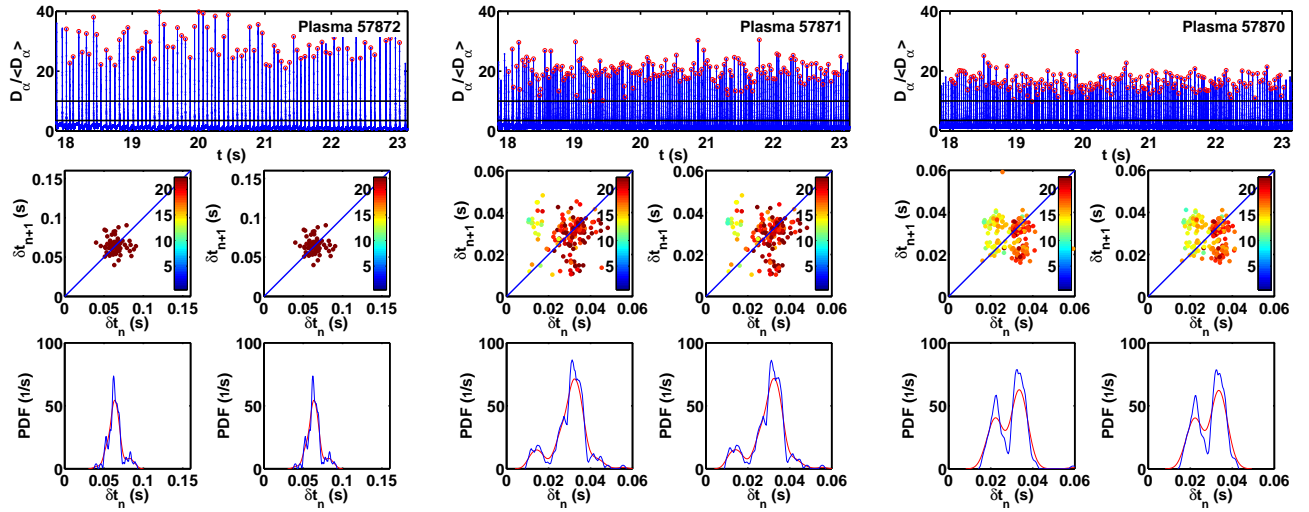


Figure 1. ELM characteristics of three similar JET plasmas 57872, 57871, 57870 at lower gas puffing rates, showing for each plasma: (top of each panel) the time trace of  $D_\alpha$  signal intensity, displaying also the two amplitude thresholds used for the centre and bottom plots; (centre of each panel) delay plots for ELMs, with amplitude colour coded above the higher (lower) threshold on the left (right); (bottom of each panel) corresponding probability density functions for the distributions of measured  $\delta t_n$  for the ELM time series, using the same amplitude thresholds as for the delay plots; the red and blue curves represent different binning of the same data. The three plasmas are ordered, from the left, in terms of increasing magnitude of gas puffing, see Fig. 3.

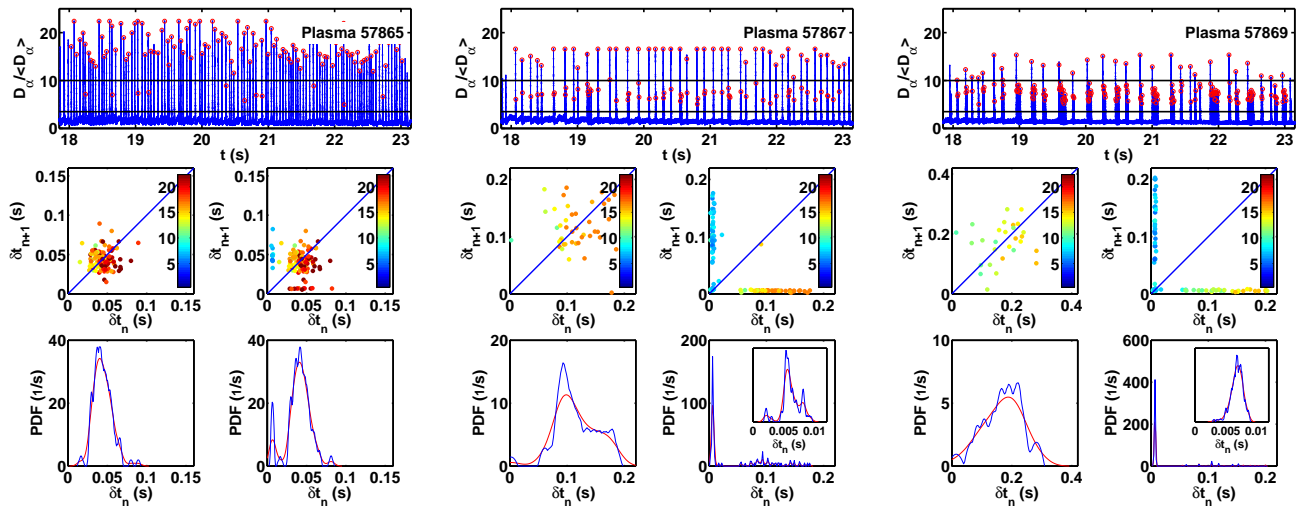


Figure 2. As Fig. 1, for three similar JET plasmas 57865, 57867, 57869 at higher gas puffing rates. The three plasmas are ordered, from the left, in terms of increasing magnitude of gas puffing, see Fig. 3. The bottom panels from JET plasmas 57867 and 57869 also include an inset panel displaying the sharp peak in the PDF. The population in this sharp peak increases with the gas puffing rate, and the average period  $\tau = 6.7 \pm 6.6 \times 10^{-2}$  (ms).

interval distribution, the distribution of the postcursors is very sharply defined and is invariant between the three JET plasmas, see Fig. 2 bottom panels. Its inverse defines a potentially important characteristic frequency of the ELMing process. This process, as seen in the delay plots, is analogous to random large amplitude transient impulses driving a system that has a narrowband reso-

nant frequency response.

Figure 3 displays the gas puffing rates for all six JET plasmas. The clear changes in ELMing displayed in Fig. 1, and for JET plasmas 57867 to 57869, arise under comparatively small changes in gas puffing, while there is a relative large step (a factor of approximately two) between 57865 and 57867. Other ELM interval dynamics

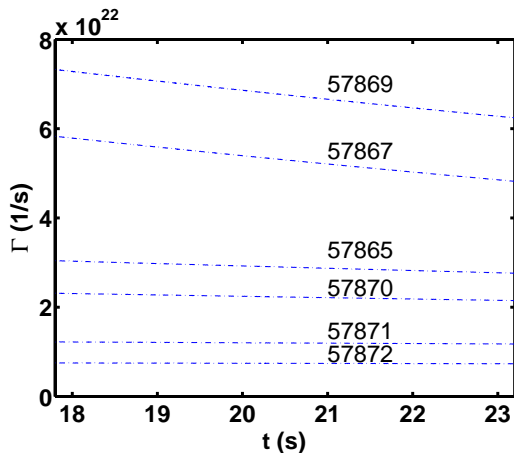


Figure 3. Time trace of gas puffing rate,  $\Gamma$ , in particles per second, which is the primary external control parameter for the six otherwise similar JET plasmas: ordered, from the bottom, in terms of increasing magnitude.

are in principle possible for other gas fuelling rates, especially for fuelling rates between those of 57865 and 57867, for these otherwise identical plasma operating regimes.

Some previous experiments have observed that Type I ELM frequency (mean inter-ELM interval) increases with gas puffing rate<sup>27</sup>. Moreover, early theoretical studies<sup>28</sup> suggested that it might be possible to explain the experimentally observed transition from Type I to Type III ELMy H-mode triggered by strong gas puffing, as well as the subsequent increase in ELM frequency and deterioration of plasma confinement, as a transition from second to first stability (either ideal or resistive modes). However, there is still no widely accepted model for the overall ELMing process or processes.

### III. SUMMARY

We have exploited the similarity of these six JET plasmas which all have exceptionally long duration  $\simeq 5$  s of the quasi-stationary ELMing process, and which appear to have only one effective control parameter, the gas puffing rate. These particular experiments yield a sufficient number of ELMs and inter-ELM times, to enable us to apply the delay plot technique to characterize the dynamics.

There exists an increasing number of ELMing regimes. These are typically characterized phenomenologically and in terms of bulk plasma parameters. We believe that ELM interval analysis of the kind presented here, if applied more widely, will help shed light on such transitions in confinement phenomenology in tokamak plasmas. In particular, demonstrating and quantifying the effectiveness of ELM control and mitigation techniques will

be assisted by characterizing the measured sequences of inter-ELM time intervals in this way.

### ACKNOWLEDGMENTS

This work, supported by the European Communities under the contract of Association between EURATOM and CCFE, was carried out within the framework of the European Fusion Development Agreement. The views and opinions expressed herein do not necessarily reflect those of the European Commission. This work was also part-funded by the RCUK Energy Programme under grant EP/I501045. We acknowledge the UK EPSRC and the Chilean committee of science and technology, CONICYT, for support.

### REFERENCES

- <sup>1</sup>M. Keilhacker, G. Becker, K. Bernhardt, A. Eberhagen, M. ElShaer, G. FuBmann, O. Gehre, J. Gernhardt, G. Gierke, E. Glock *et al.*, Plasma Phys. Controlled Fusion **26**, 49 (1984).
- <sup>2</sup>V. Erckmann, F. Wagner, J. Baldzuhn, R. Brakel, R. Burhenn, U. Gasparino, P. Grigull, H. J. Hartfuss, J. V. Hofmann, R. Jaenicke *et al.*, Phys. Rev. Lett. **70**, 2086 (1993).
- <sup>3</sup>H. Zohm, Plasma Phys. Controlled Fusion **38**, 105 (1996).
- <sup>4</sup>A. Loarte, G. Saibene, R. Sartori, D. Campbell, M. Becoulet, L. Horton, T. Eich, A. Herrmann, G. Matthews, N. Asakura *et al.*, Plasma Phys. Controlled Fusion **45**, 1549 (2003).
- <sup>5</sup>K. Kamiya, N. Asakura, J. Boedo, T. Eich, G. Federici, M. Fenstermacher, K. Finken, A. Herrmann, J. Terry, A. Kirk *et al.*, Plasma Phys. Controlled Fusion **49**, S43 (2007).
- <sup>6</sup>R. J. Hawryluk, D. J. Campbell, G. Janeschitz, P. R. Thomas, R. Albanese, R. Ambrosino, C. Bachmann, L. Baylor, M. Becoulet, I. Benfatto *et al.*, Nucl. Fusion **49**, 065012 (2009).
- <sup>7</sup>T. E. Evans, R. A. Moyer, K. H. Burrell, M. E. Fenstermacher, I. Joseph, A. W. Leonard, T. H. Osborne, G. D. Porter, M. J. Schaffer, P. B. Snyder *et al.*, Nat. Phys. **2**, 419 (2006).
- <sup>8</sup>Y. Liang, H. R. Koslowski, P. R. Thomas, E. Nardon, B. Alper, P. Andrew, Y. Andrew, G. Arnoux, Y. Baranov, M. Bécoulet *et al.*, Phys. Rev. Lett. **98**, 265004 (2007).
- <sup>9</sup>A. Kirk, J. Harrison, Y. Liu, E. Nardon, I. T. Chapman and P. Denner (the MAST team), Phys. Rev. Lett. **108**, 255003 (2012).
- <sup>10</sup>A. W. Degeling, Y. R. Martin, P. E. Bak, J. B. Lister and X. Llobet, Plasma Phys. Controlled Fusion **43**, 1671 (2001).
- <sup>11</sup>J. Greenhough, S. C. Chapman, R. O. Dendy and D. J. Ward, Plasma Phys. Controlled Fusion **45**, 747 (2003).
- <sup>12</sup>S.-I. Itoh, K. Itoh, A. Fukuyama and Y. Miura, Phys. Rev. Lett. **67**, 2485 (1991).
- <sup>13</sup>D. Ruelle and F. Takens, Commun. Math. Phys. **20**, 167 (1971).
- <sup>14</sup>S. Newhouse, D. Ruelle and F. Takens, Commun. Math. Phys. **64**, 35 (1978).
- <sup>15</sup>L. N. Trefethen, A. E. Trefethen, S. C. Reddy and T. A. Driscoll, Science **261**, 578 (1993).
- <sup>16</sup>E. Bodenschatz, W. Pesch and G. Ahlers, Annu. Rev. Fluid Mech. **32**, 709 (2000).
- <sup>17</sup>G. Ahlers, Phys. Rev. Lett. **33**, 1185 (1974).
- <sup>18</sup>J. P. Gollub and H. L. Swinney, Phys. Rev. Lett. **35**, 927 (1975).
- <sup>19</sup>J. P. Gollub and S. V. Benson, J. Fluid Mech. **100**, 449 (1980).
- <sup>20</sup>A. Libchaber, S. Fauve and C. Laroche, Physica D **7**, 73 (1983).
- <sup>21</sup>T. Klinger, A. Latten, A. Piel, G. Bonhomme, T. Pierre and T. Dudok de Wit, Phys. Rev. Lett. **79**, 3913 (1997).
- <sup>22</sup>F. Brochard, E. Gravier and G. Bonhomme, Phys. Rev. E **73**, 036403 (2006).



- <sup>23</sup>S. K. Matsoukis, S. Chapman and G. Rowlands, *Physica D* **138**, 251 (2000).
- <sup>24</sup>P. E. Devine and S. C. Chapman, *Physica D* **95**, 35 (1996).
- <sup>25</sup>T. Schreiber and A. Schmitz, *Physica D* **142**, 346 (2000).
- <sup>26</sup>J. Pamela, J. Ongena and J. E. Contributors, *Nucl. Fusion* **45**, S63 (2005).
- <sup>27</sup>D. C. McDonald, Y. Andrew, G. T. A. Huysmans, A. Loarte, J. Ongena, J. Rapp and S. Saarelma, *Fusion Sci. Technol.* **53**, 891 (2008).
- <sup>28</sup>J.-S. Lönnroth, V. V. Parail, G. Corrigan, D. Heading, G. Huysmans, A. Loarte, S. Saarelma, G. Saibene, S. Sharapov, J. Spence *et al.*, *Plasma Phys. Controlled Fusion* **45**, 1689 (2003).